Structural and electronic properties of the Bi/Au(110)–1×4 surface

A. Crepaldi,[1] C. Tournier-Colletta,[1,*] M. Pivetta,[1] G. Autès,[2] F. Patthey,[1] H. Brune,[1] O. V. Yazyev,[2] and M. Grioni[1]
[1]*Institute of Condensed Matter Physics, Ecole Polytechnique Fédérale de Lausanne (EPFL), CH-1015 Lausanne, Switzerland*
[2]*Institute of Theoretical Physics, Ecole Polytechnique Fédérale de Lausanne (EPFL), CH-1015 Lausanne, Switzerland*
(Received 6 September 2013; revised manuscript received 17 October 2013; published 26 November 2013)

We report on the structural and electronic properties of the Bi/Au(110)–1 × 4 surface, by combining scanning tunneling microscopy, angle-resolved photoemission spectroscopy, and first-principles calculations. The analysis of the precursor 1 × 8 moiré structure shows that the 1 × 4 reconstruction forms at an optimum coverage of one monolayer. A hard-sphere model is proposed for the 1 × 4 structure and further confirmed by calculations. In this model, topmost Bi atoms form rows supported by a Bi overlayer, with no significant alloying with the substrate. This has important consequences regarding the electronic properties and the spin texture. The photoemission measurements evidence typical *p* Bi-induced states, that can have either quasi-one- or two-dimensional character depending on their binding energy. These states show no Rashba spin splitting, in agreement with the results of first-principles calculations. This finding is discussed by considering the role of hybridization with the substrate in the emergence of the Rashba effect.

DOI: 10.1103/PhysRevB.88.195433 PACS number(s): 73.20.At, 68.37.Ef, 74.25.Jb, 71.15.Mb

I. INTRODUCTION

In the context of emergent spintronic devices, materials exhibiting the Rashba effect play an important role. Thanks to their spin-split electronic states, these materials can in fact carry spin-polarized currents. The Rashba effect originates from the lifting of the Kramers spin degeneracy by the spin-orbit (SO) interaction in systems with broken inversion symmetry. The latter condition can be fulfilled either at surfaces (Rashba-Bychkov effect[1]) or in the bulk of noncentrosymmetric crystals as originally proposed by Dresselhaus and Rashba.[2,3]

The strength of the Rashba coupling α_R is a fundamental parameter since it determines the spin precession length.[4] It is thus highly desirable to find new materials exhibiting the so-called giant Rashba effect characterized by large values of α_R. So far, the largest ever reported α_R are for the Bi/Ag(111) surface alloy[5] ($\alpha_R \approx 3$ eV Å) and the surface states of the noncentrosymmetric compound BiTeI[6–9] ($\alpha_R \approx 4$ eV Å). Three main ingredients, whose respective contributions cannot be trivially disentangled, are important to produce the giant Rashba effect: (i) a large atomic SO parameter as found in high-Z elements such as Bi, (ii) a large perpendicular potential gradient,[10,11] and finally (iii) a large in-plane potential gradient, as realized by the buckling of high-Z atoms in surface alloys.[12–14] The latter two can be unified by introducing the concept of wave function asymmetry stemming from the mixture of the adsorbate and the substrate atomic orbitals.

Another issue, so far not extensively investigated, is the dimensionality aspect. The examples mentioned previously are 2D electron gases, but can one transpose the giant Rashba effect to one-dimensional systems to produce perfectly directed spin currents? Quasi-one-dimensional systems are also interesting to test the predictions of theoretical models, such as the extended Rashba model that includes a large in-plane asymmetry. The first realization of a spin-split, one-dimensional electron gas was obtained in Au wires grown on stepped silicon.[15,16] However, the Rashba parameter remains small, of the order of what is found for the Au(111) Shockley state[17] ($\alpha_R = 0.33$ eV Å). A significantly larger Rashba effect has recently been observed for Pt nanowires on the Si(110) surface.[18] Finally, one-dimensional Rashba systems could exhibit novel transport properties, for instance a one-dimensional spin Hall effect as proposed in stepped $Bi_{0.9}Sb_{0.1}$(114).[19]

In this paper, we report on the atomic and electronic structure of the Bi/Au(110) surface, a system of fundamental interest where both adsorbate and substrate are composed of high-Z elements conducive to a significant Rashba effect. Moreover, the (110) surface is a good template candidate for the growth of quasi-1D nanostructures.[20] A wide variety of reconstructions at Bi coverages below one monolayer (ML) is observed with scanning tunneling microscopy (STM).[21] We focus here on the 1 × 8 moiré structure (0.875 ML) and, more importantly, on the 1 × 4 surface reconstruction obtained at 1 ML coverage. Starting from the moiré structure, we propose a hard-sphere model for the 1 × 4 surface corroborated by DFT calculations. The electronic structure of the surface has been measured by means of angle-resolved photoemission spectroscopy (ARPES). Characteristic Bi-induced states are observed, showing either quasi-one- or two-dimensional contours depending on their binding energy. No spin-splitting is reported, in agreement with the theoretical predictions. The absence of Rashba effect is finally discussed in terms of hybridization with the substrate.

II. EXPERIMENT

STM and ARPES experiments have been performed in two different UHV setups. The STM experiments have been carried out in a home-built scanning tunneling microscope operated at 5 K.[22] We used chemically etched tungsten tips. The indicated tunnel voltages V_t correspond to the sample potential. For the ARPES experiments, we used a high-brightness Gammadata VUV 5000 helium discharge lamp, monochromatized at the Iα emission line ($h\nu = 21.21$ eV). ARPES measurements were performed at 77 K using a SPECS Phoibos 150 hemispherical analyzer. Energy and momentum resolutions were set to 10 meV and 0.3°, respectively. Low-energy electron diffraction (LEED) measurements have been performed at

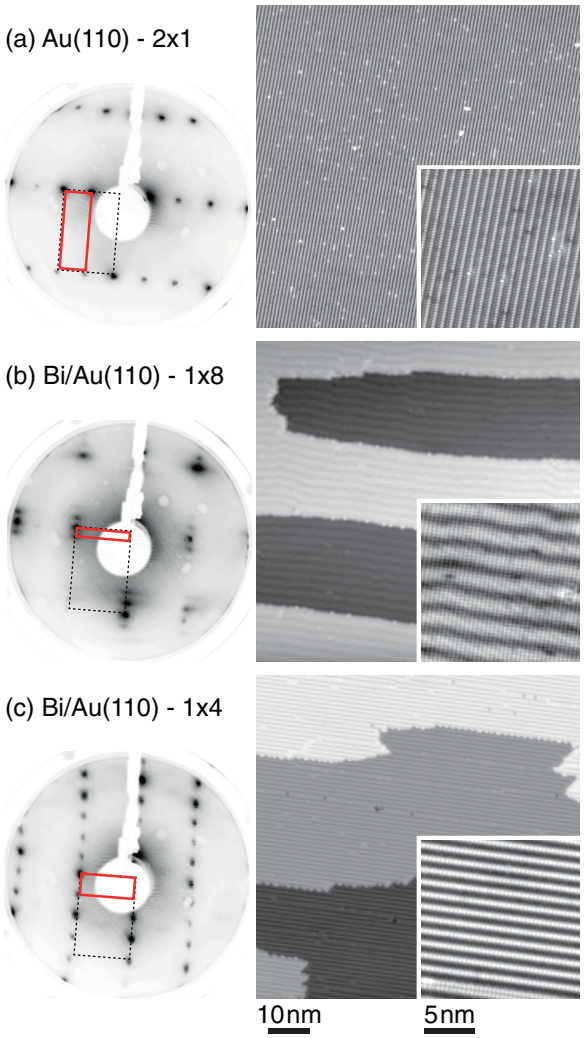

FIG. 1. (Color online) Surface reconstructions of the Bi/Au(110) surface for increasing Bi coverage θ: (a) pristine Au(110)–2×1 surface, (b) Bi/Au(110)–1×8 surface ($\theta = 0.875$ ML), and (c) Bi/Au(110)–1×4 surface ($\theta = 1$ ML). The corresponding LEED patterns (left) are measured at 50 eV; unit cells in k space are enclosed by red lines (dotted black is the non-reconstructed 1×1 surface). Large-scale and close-up STM images (right) cover 78×78 nm^2 and 15.6×15.6 nm^2 areas, respectively. The tunneling parameters are $V_t = -20$ mV, $I_t = 0.02$ nA for the large-scale images and $V_t = -10$ mV, $I_t = 10$ nA for the small-scale images.

room temperature in both setups to correlate the STM and ARPES data.

The Au(110) substrate was prepared by standard Ar^+ sputtering/annealing cycles, to produce a high-quality 2×1–reconstructed surface as indicated by sharp spots in the LEED patterns and wide, almost defect-free terraces in the STM images [Fig. 1(a)]. The 2×1 surface exhibits the so-called "missing row" reconstruction[23] with intra- and interchain spacings $a/\sqrt{2} = 2.88$ Å and $2a = 8.16$ Å, respectively [Fig. 2(a)]. Bi was evaporated either from a standard Knudsen cell (STM) or from a calibrated EFM3 Omicron evaporator (ARPES), onto a freshly prepared substrate kept at room temperature.

First-principles electronic structure calculations have been performed within the density functional theory (DFT) framework employing the generalized gradient approximation (GGA) as implemented in the QUANTUM-ESPRESSO package.[24] Spin-orbit effects were accounted for using the fully relativistic norm-conserving pseudopotentials acting on valence electron wave functions represented in the two-component spinor form.[25]

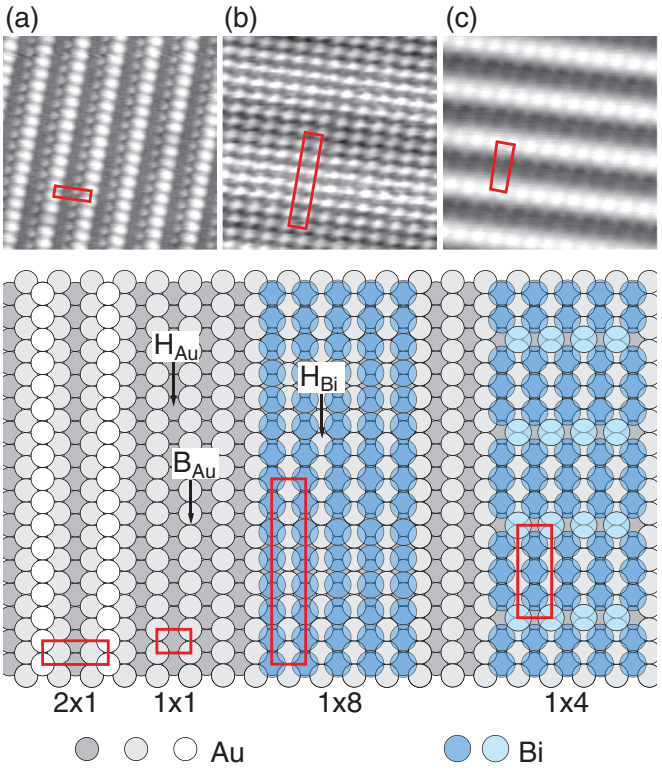

FIG. 2. (Color online) Atomically resolved STM images of (a) Au(110)–2×1 missing-row reconstruction, (b) Bi/Au(110)–1×8 moiré structure, and (c) Bi/Au(110)–1×4 surface. Unit cells are depicted in red. STM images covering 5×5 nm^2 area have been acquired with typical tunneling parameters $V_t = -5$ mV and $I_t = 10$ nA. Lower panel: hard sphere models; H_{Au}, H_{Bi}, and B_{Au} refer to hollow Au and Bi sites and bridge sites, respectively.

III. SURFACE RECONSTRUCTIONS OF THE Bi/Au(110) SURFACE

Upon Bi adsorption, the native 2×1 reconstruction is replaced by a variety of new reconstructions at coverages below one monolayer (ML, defined as one Bi atom per 1×1 unit cell). A description of these phases goes beyond the scope of this paper and will be presented elsewhere.[21] We just mention here the occurrence of the quasihexagonal $c(2 \times 2)$ and $(\sqrt{3} \times \sqrt{3})R54.7^\circ$ reconstructions at 1/2 ML and 1/3 ML, respectively, as already observed for similar interfaces.[26–28]

For higher coverages, one-dimensional structures, rotated by 90° with respect to the "missing row" reconstruction, are observed [Figs. 1(b) and 1(c)]. The first structure we consider is the 1×8 moiré surface, that appears as a one-dimensional modulation of the atomic heights, with amplitude $\delta_z \approx 15$ pm. The atomically resolved images [Fig. 2(b)] yield an interatomic spacing $d_{Bi-Bi} = 3.29$ Å, that matches exactly the average of the first- and second-neighbor distances ($d_1 = 3.062$ Å

and $d_2 = 3.512$ Å) found in rhombohedral bulk Bi.[29] This typical value also appears in the incommensurate phase of Bi/Cu(111) forming at high coverages.[30] A dense packing of Bi atoms, as in the previously cited system, is compatible with the 1×8 structure. Furthermore, we count seven atoms per 1×8 unit cell. Therefore, the observed stripes are rationalized easily as a moiré effect. Indeed, given the Au-Au separation at the Au(110)–1×1 surface ($d_{\mathrm{Au-Au}} = a/\sqrt{2} = 2.88$ Å), one finds out that eight Au atoms can effectively accommodate seven densely packed Bi atoms ($8 \times d_{\mathrm{Au-Au}} = 23.04$ Å; $7 \times d_{\mathrm{Bi-Bi}} = 23.03$ Å). The resulting coverage is then $7/8 = 0.875$ ML. A hard-sphere model for the 1×8 moiré structure is shown in Fig. 2(b). The lowest Bi adatoms occupy hollow sites H_{Au} and define the corners of the unit cell. The other atoms of the cell are progressively shifted away from hollow sites due to the mismatch between Bi and Au radii, resulting in higher atomic heights at the center of the cell. Finally, undulations of the moiré pattern in the perpendicular direction [see inset, Fig. 1(b)] are a likely consequence of the steps morphology. Such shifts perpendicular to the steps do not modify the moiré energy because of the large number of densely packed atoms in the unit cell.

At an optimum coverage of 1 ML, the 1×4 structure is observed[38] [Fig. 1(c)]. Its main feature is the formation of straight, bright lines assigned to Bi rows. The 1×4 surface does not show the typical undulations observed in the moiré structure. Given that the row atoms occupy preferential sites, it is indeed energetically unfavorable to shift the structure perpendicular to the steps. The transition from the 1×8 moiré structure to the 1×4 surface for intermediate coverages is documented elsewhere.[21] We just mention that the formation of Bi rows is dictated by "magical distances" between the latter, in order to preserve the moiré pattern within rows. A hard-sphere model is also proposed for the 1×4 structure [Fig. 2(c)]. Besides the corner atoms (Bi_1) pertaining to the rows, the 1×4 unit cell comprises three inner (Bi_2, Bi_3, and Bi_4), densely packed Bi atoms occupying H_{Au} sites. This gives four atoms in the 1×4 cell, hence a coverage of 1 ML. In the STM image, only top Bi_1 (bright) and inner Bi_2 (faint) atoms are observed. An estimate of the height difference gives $\delta_z \approx 60$ pm.

The 1×4 surface periodicity is also found at the systems formed by heavy atoms (Bi, Pb) deposited on the Cu(110) surface,[27,31] so one could have naively proposed the same structure. In the latter, topmost heavy atoms adopt a double-row structure, separated by grooves where Bi substitute Cu atoms and thus implying a significant alloying. However, in the Bi/Au(110) system alloying is unlikely because Bi and Au are essentially nonmiscible in the bulk.[32] In addition, the recently discovered Bi/Au(111)–6×6 phase shows no alloying but an overlayer structure.[33]

TABLE I. Relaxed atomic positions of the Bi/Au(110)–1×4 structure obtained from first-principles calculations.

	x (Å)	y (Å)	z (Å)
Bi_1	0.0000	0.0000	0.0000
Bi_2	2.0982	2.5393	−0.8328
Bi_3	2.0982	5.9357	−0.9302
Bi_4	2.0982	9.3301	−0.8328
Au_1	0.0000	1.4516	−2.5788
Au_2	0.0000	4.4230	−2.4463
Au_3	0.0000	7.4145	−2.4463
Au_4	0.0000	10.3537	−2.5788

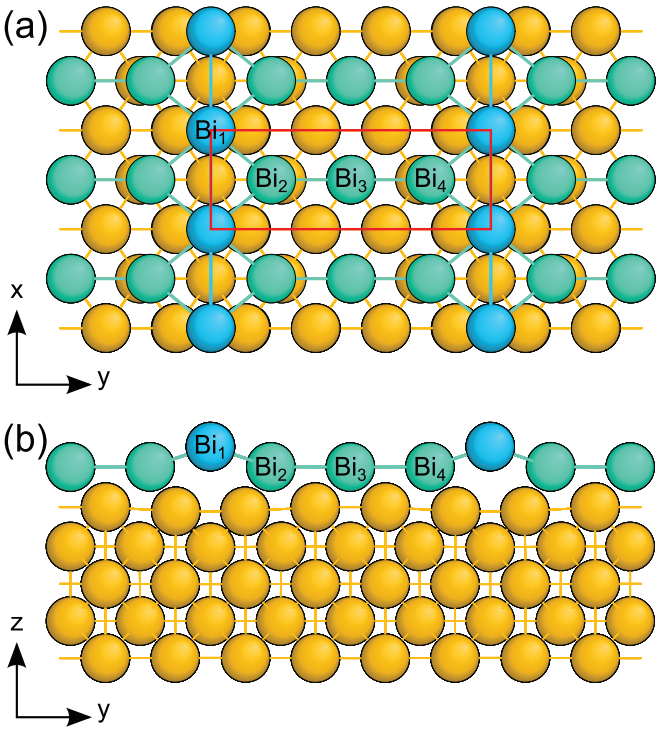

FIG. 3. (Color online) (a) Top view and (b) side view of relaxed atomic structure of the Bi/Au(110)–1×4 surface obtained from first-principles calculations. The 1×4 unit cell is depicted in red. First two Au layers are shown. Bi and Au atoms are depicted in blue/green and yellow, respectively.

Our first-principles calculations confirm that the proposed structure for the 1×4 system is a stable configuration. We considered a slab model of 15 Au(110) atomic layers in a 1×4 supercell terminated on both sides by a Bi monolayer. The structure was fully relaxed. The coordinates of Bi atoms and Au atoms in the first layer are listed in Table I. The Bi_1 atoms (blue in Fig. 3) occupy the topmost hollow sites H_{Bi} and form the rows described previously, running along the x direction. Each Bi_1 atom is coordinated to four Bi_2 and Bi_4 atoms (green) that are significantly shifted into the surface ($\delta z = -0.83$ Å). The central atom Bi_3 is displaced downwards even more ($\delta z = -0.93$ Å). It is interesting to note that the relaxed positions of the Bi_2 and Bi_4 atoms deviate from their initial H_{Au} positions. Indeed, we observe a distinct shift towards the rows ($\delta y = \pm 0.45$ Å) that is easily noticed by the mismatch with atoms from the second Au layer. This corroborates our hard-sphere model since in this configuration Bi atoms are separated by the same distance $d_{\mathrm{Bi_2-Bi_3}} = d_{\mathrm{Bi_1-Bi_2}} = 3.40$ Å that approaches the average of first- and second-neighbor distances in bulk Bi.

IV. ELECTRONIC STRUCTURE OF THE 1 × 4 SURFACE RECONSTRUCTION

In the following, we analyze the electronic structure of the Bi/Au(110)–1×4 surface, motivated by the possibility of having quasi-one-dimensional Rashba states supported by the

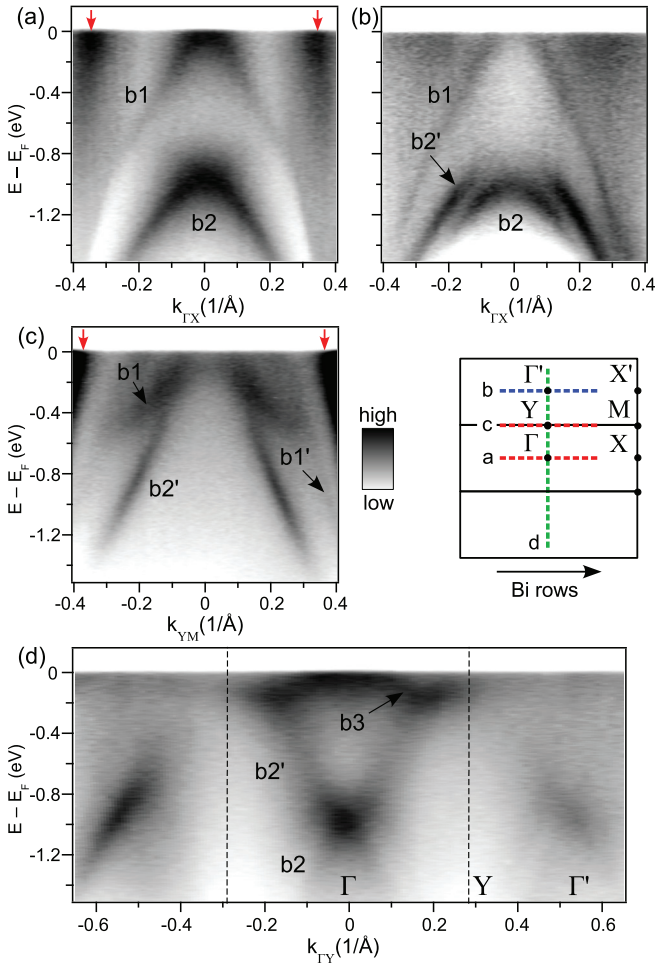

FIG. 4. (Color online) ARPES intensity maps measured for the Bi/Au(110)–1 × 4 surface along high-symmetry directions $\Gamma-X$ [(a) first SBZ, (b) second SBZ], $Y-M$ (c), and $\Gamma-Y$ (d). The red, vertical arrows indicate bulk states. Surface Brillouin zones and the segments probed by ARPES are indicated.

Bi rows. Figure 4 shows ARPES intensity maps measured along the surface high-symmetry directions. Surface Brillouin zones (SBZs) are indicated in the figure. For clarity, we give the zone boundary wave vectors: $\Gamma Y = 0.273$ Å^{-1} and $\Gamma X = YM = 0.770$ Å^{-1}. Along the chain direction $\Gamma-X$ we observe two strongly dispersing features $b1$ and $b2$ with negative effective mass [Fig. 4(a)]. This is a common feature of Bi-induced states of p character. The intense features indicated by red arrows are sp-type bulk states of the Au(110)–2 × 1 substrate.[34] The surface is metallic as demonstrated by the $b1$ state crossing the Fermi level. This feature is more clearly seen in the second SBZ [Fig. 4(b)]. An additional band $b2'$ is also visible, which is instead absent in the first SBZ due to matrix-element effects.[35] The $b2'$ state disperses similarly to $b2$ with comparable effective mass, but shifted to lower binding energies. At first glance $b2$ and $b2'$ look alike spin-split states, but calculations will discard that possibility. Along the inequivalent chain direction $Y-M$ [Fig. 4(c)], one recognizes the previously discussed $b1$ and $b2'$ states, the latter being shifted to lower binding energies due to the positive dispersion perpendicular to the Bi rows [Fig. 4(d)]. Along $Y-M$, a new state $b1'$ with negative effective mass is observed. This state is actually degenerate with $b1$ along $\Gamma-X$ and then splits off when moving to $Y-M$.

Along the $\Gamma-Y$ direction perpendicular to the chains we first notice the $b2$ band, already evidenced along the $\Gamma-X$ direction, with minimum binding energy 1 eV at the Γ point [Fig. 4(d)]. The effective mass of this band is comparable to the one observed along $\Gamma-X$, suggesting its quasi-two-dimensional character. As mentioned before, the effective mass of the $b2'$ state becomes positive along $\Gamma-Y$, resulting in a saddle point at Γ. At 0.2 eV below the Fermi level $b2$ meets new band $b3$. The latter has a small bandwidth and forms a hole pocket centered at the Γ point.

Figure 5 compares ARPES measurements to the band structure calculated from first principles. The experimental band dispersions (black dots) have been extracted from the intensity maps shown in Fig. 4 after Laplacian filtering. The size and color of the symbols superimposed on calculated bands indicates the projected weight on the topmost layer of Bi atoms. There is an overall good agreement between experiment and theory. According to the calculations, the bands that fit the experimental dispersions are strongly localized at the surface (except $b4$ that matches with a group of bulk states). The strong surface character explains the large intensity observed in the experiment. Our calculations show that all bands are spin-degenerate; hence no sizable Rashba effect occurs at the Bi/Au(110)–1 × 4 interface despite the high atomic number of its atomic constituents.

We turn now to the analysis of constant-energy (CE) maps. Figures 5(b)–5(d) reveal that depending on binding energy the electronic states are either of one- or two-dimensional character. Overall, the calculated CE maps [Figs. 5(e)–5(g)] reproduce well the observed features. At high binding energy ($E_B = 1.2$ eV), the overall symmetry of the experimental CE map is two-dimensional, with two circular contours centered at Y. The calculated contours are somewhat wider due to the slight mismatch with the experimental effective mass at high binding energies. In a nearly free electron model, these contours would stem from a parabolic band that is replicated due to the interrow potential by the wave vector $\vec{Q}_\perp = 2\vec{\Gamma Y}$. At this particular energy, the two contours overlap and a close inspection reveals that they interact, or alternatively that a gap opens due to a weak Fourier component $V_{\vec{Q}_\perp}$. This leads to the formation of inner, ellipsoidal and outer, sinelike contours associated with $b2$ and $b2'$, respectively. The contours of the Au bulk states (red arrows) show wigglings similar to $b2'$, that again reflects the surface periodicity as already observed on the Au(100)–2 × 1 surface.[34]

At lower binding energies, the two-dimensional symmetry is progressively lost [Figs. 5(c)–5(d)]. In particular, at $E_B = 0.7$ eV, a quasi-one-dimensional contour associated with $b1$ emerges from the Au bulk states (see white arrow). The contours of the replicated bands discussed previously shrink at lower binding energy because of the effective mass. The replicated contours no longer interact, and therefore keep their circular shape. One ends up with one contour per SBZ, assigned to $b2'$. Close to the Fermi level ($E_B = 0.2$ eV), the experimental CE map shows rather straight lines running along the $\Gamma-Y$ direction, demonstrating the predominance of quasi-one-dimensional states. By a close inspection of the band topology, we disentangle three contributions: small hole

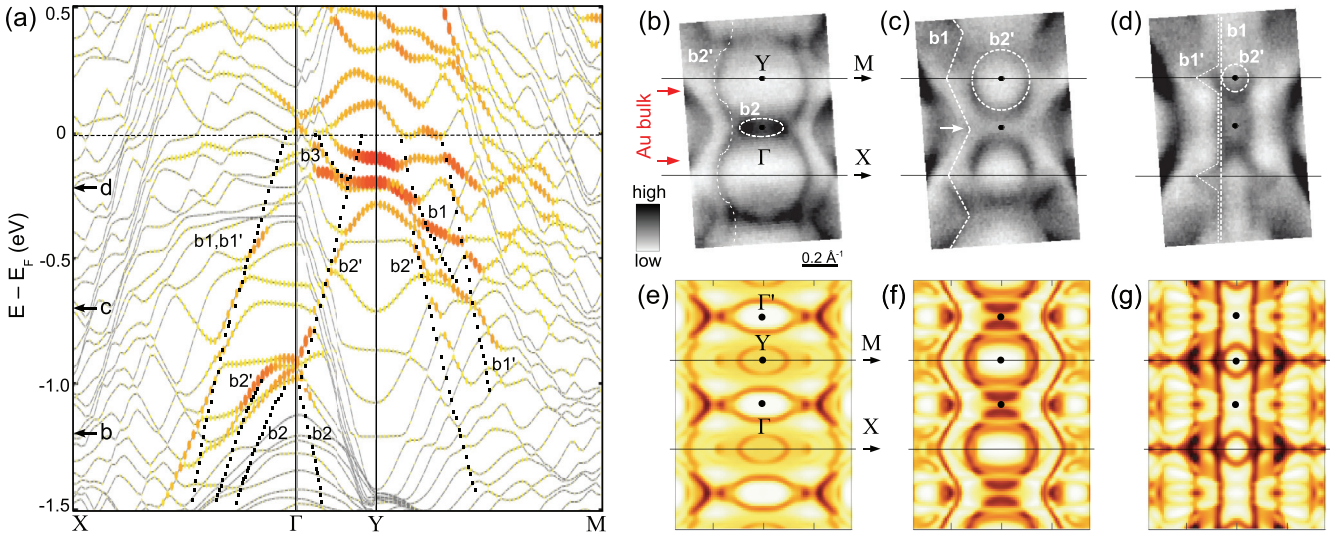

FIG. 5. (Color online) First-principles band structure of the slab model of Bi/Au(110)–1 × 4 surface plotted along high-symmetry k-point path X–Γ–Y–M. The size of the symbols represents the projected weight on Bi atoms. Black dots indicate the experimental band dispersions obtained from data in Fig. 3. Experimental constant-energy (CE) maps are measured at (b) 1.2 eV, (c) 0.7 eV, and (d) 0.2 eV binding energies. (e)–(g) Corresponding CE maps calculated from first-principles, projected on the Bi atoms. Dotted lines are guides to the eye emphasizing the symmetry of the contours.

pockets centered at Y ($b2'$), flat segments with shark-fin-shaped features forming close to Y ($b1'$, dotted line), and almost flat segments ($b1$, dashed line). The latter are not observed at higher binding energy because $b1'$ essentially overlaps with $b1$ along both Γ–X and Y–M [see Fig. 5(a)]. However close to E_F, $b1'$ shows a larger k value along Y–M than $b1$, that accounts for the shark-fin feature.

The change from one- to two-dimensional character can be rationalized by examining the calculated local density of states (LDOS). Figure 6(a) shows the LDOS corresponding to the electronic state located at Y and $E_B \simeq 0.1$ eV [see Fig. 5(a)]. The wave function is mainly localized on the Bi_1 row atoms and is mainly composed of p_x orbitals pointing along the row direction. A much smaller contribution arises from neighboring Bi_2 and Bi_4 atoms. However, no weight is found on central atoms Bi_3. In Fig. 6(b) we show the LDOS in the plane perpendicular to the Bi rows, and integrated along the latter. It is obvious here that adjacent Bi_1 rows are decoupled from an electronic point of view, as demonstrated by the absence of weight on Bi_3 atoms, but also by the vanishing hybridization of Bi overlayer with Au atoms located below Bi_3. This corroborates the 1D character of the lower energy states.

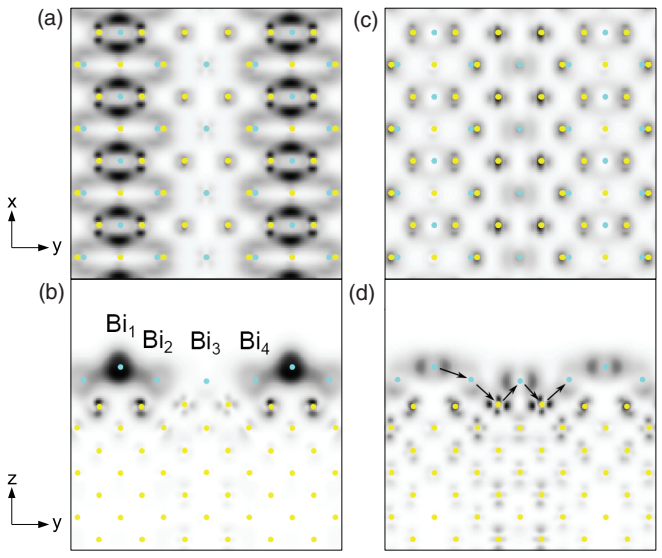

FIG. 6. (Color online) Local electron density plots of 1D (a) and 2D (c) states calculated at points Y and Γ, respectively. The density integrated along the Bi chains is shown in (b) and (d). The arrows represent the effective hopping mechanism between Bi rows.

The spatial distribution of electronic states changes at higher binding energy [Fig. 6(c), $E_B \simeq 1$ eV at the Γ point]. Indeed, significant weight is found on both the topmost Bi_1 and the central Bi_3 atoms. Here, the wave function is mainly of p_y character, with lobes perpendicular to the row direction. In the integrated LDOS plot we point out a strong hybridization between between Bi and Au atoms [Fig. 6(d)]. Within the tight-binding approach, an effective hopping scheme between Bi rows can be proposed as follows: $Bi_1 \rightarrow Bi_2 \rightarrow Au \rightarrow Bi_3 \rightarrow Au \rightarrow Bi_2 \rightarrow Bi_1$ [arrows in Fig. 6(d)]. Judging on the almost isotropic CE maps, this effective hopping mechanism has to be of the same magnitude as the intrachain hopping to produce a 2D-like dispersion.

With the help of LDOS plots one can finally address qualitatively the absence of spin splitting of the surface states. While the interaction with the substrate has just been shown to be nonnegligible and responsible for the interchain hopping, it is actually not sufficient to produce a strong asymmetry of the wave function near the ion cores. Indeed, as can be seen in Fig. 6(d), the contributions from Bi_1 and Bi_3 atoms closely resemble the atomic p_y orbitals. This is at odds with the strong asymmetries reported in Rashba surface alloys.[11] In the Bi/Au(110)–1 × 4 system, the topmost Bi_1 atoms are never coupled to the substrate, but hybridize only with the Bi_2

atoms without any noticeable deviation from the p_y shape. On the other hand, Bi_3 atoms do couple to the substrate but again without inducing any strong asymmetry.

In the Bi(Pb)/Ag(111) systems, surface alloying has been pointed out to be the crucial requirement for triggering the giant Rashba effect, because it (i) induces a strong in-plane potential gradient[13] and (ii) is generally accompanied by a buckling of the heavy atoms.[14] Both conditions favor the asymmetry of the wave function because the Bi p_z and the substrate in-plane $p_{x,y}$ orbitals strongly hybridize. By contrast, no alloying occurs at the 1 ML Pb/Au(111) moiré structure and no Rashba effect has been reported.[36] In the Bi/Au(110)–1 × 4 system, although the substrate symmetry is different and the relevant Bi orbitals have rather $p_{x,y}$ character, we believe that alloying with the substrate is also required to have a sizable spin splitting. This assumption is confirmed by the striking contrast between the Bi/Au(110)–1 × 4 surface overlayer system and the Bi/Cu(110)–1 × 4 surface alloy that instead shows spin-split states.[37] The comparison points to the important role of the substrate, namely the fact that gold does not favor alloying.

V. CONCLUSION

The structural and electronic properties of the 1 ML Bi/Au(110)–1 × 4 interface have been studied in detail by means of STM, ARPES, and DFT calculations. The interface supports quasi-one-dimensional states at low energy, localized on the Bi rows. However, the electronic states acquire a more two-dimensional character with increasing binding energy, with the Bi rows becoming significantly hybridized. The Bi/Au(110) surface does not exhibit any sizable spin splitting due to the lack of surface alloying and the consequent absence of asymmetry of the wave function, in sharp contrast with the recently studied Bi/Cu(110) surface alloy.

ACKNOWLEDGMENTS

G.A. and O.V.Y. were supported by the Swiss National Science Foundation (Grant No. PP00P2_133552) and by the ERC Starting Grant "TopoMat" (Grant No. 306504). First-principles computations have been performed at the Swiss National Supercomputing Centre (CSCS) under Project No. s443.

*cedric.tournier@epfl.ch

[1] Y. A. Bychkov and E. I. Rashba, JETP Lett. **39**, 78 (1984).
[2] G. Dresselhaus, Phys. Rev. **100**, 580 (1955).
[3] E. I. Rashba, Sov. Phys. Solid State **2**, 1109 (1960).
[4] S. Datta and B. Das, Appl. Phys. Lett. **56**, 665 (1990).
[5] C. R. Ast, J. Henk, A. Ernst, L. Moreschini, M. C. Falub, D. Pacilé, P. Bruno, K. Kern, and M. Grioni, Phys. Rev. Lett. **98**, 186807 (2007).
[6] K. Ishizaka, M. S. Bahramy, H. Murakawa, M. Sakano, T. Shimojima, T. Sonobe, K. Koizumi, S. Shin, H. Miyahara, A. Kimura, K. Miyamoto, T. Okuda, H. Namatame, M. Taniguchi, R. Arita, N. Nagaosa, K. Kobayashi, Y. Murakami, R. Kumai, Y. Kaneko, Y. Onose, and Y. Tokura, Nat. Mater. **10**, 521 (2011).
[7] A. Crepaldi, L. Moreschini, G. Autès, C. Tournier-Colletta, S. Moser, N. Virk, H. Berger, Ph. Bugnon, Y. J. Chang, K. Kern, A. Bostwick, E. Rotenberg, O. V. Yazyev, and M. Grioni, Phys. Rev. Lett. **109**, 096803 (2012).
[8] G. Landolt, S. V. Eremeev, Y. M. Koroteev, B. Slomski, S. Muff, T. Neupert, M. Kobayashi, V. N. Strocov, T. Schmitt, Z. S. Aliev, M. B. Babanly, I. R. Amiraslanov, E. V. Chulkov, J. Osterwalder, and J. H. Dil, Phys. Rev. Lett. **109**, 116403 (2012).
[9] M. Sakano, M. S. Bahramy, A. Katayama, T. Shimojima, H. Murakawa, Y. Kaneko, W. Malaeb, S. Shin, K. Ono, H. Kumigashira, R. Arita, N. Nagaosa, H. Y. Hwang, Y. Tokura, and K. Ishizaka, Phys. Rev. Lett. **110**, 107204 (2013).
[10] S. Mathias, A. Ruffing, F. Deicke, M. Wiesenmayer, I. Sakar, G. Bihlmayer, E. V. Chulkov, Yu. M. Koroteev, P. M. Echenique, M. Bauer, and M. Aeschlimann, Phys. Rev. Lett. **104**, 066802 (2010).
[11] H. Bentmann, T. Kuzumaki, G. Bihlmayer, S. Blügel, E. V. Chulkov, F. Reinert, and K. Sakamoto, Phys. Rev. B **84**, 115426 (2011).
[12] G. Bihlmayer, S. Blügel, and E. V. Chulkov, Phys. Rev. B **75**, 195414 (2007).
[13] J. Premper, M. Trautmann, J. Henk, and P. Bruno, Phys. Rev. B **76**, 073310 (2007).
[14] I. Gierz, B. Stadtmüller, J. Vuorinen, M. Lindroos, F. Meier, J. H. Dil, K. Kern, and C. R. Ast, Phys. Rev. B **81**, 245430 (2010).
[15] D. Sànchez-Portal, S. Riikonen, and R. M. Martin, Phys. Rev. Lett. **93**, 146803 (2004).
[16] I. Barke, F. Zheng, T. K. Rügheimer, and F. J. Himpsel, Phys. Rev. Lett. **97**, 226405 (2006).
[17] S. LaShell, B. A. McDougall, and E. Jensen, Phys. Rev. Lett. **77**, 3419 (1996).
[18] J. Park, S. W. Jung, M.-C. Jung, H. Yamane, N. Kosugi, and H. W. Yeom, Phys. Rev. Lett. **110**, 036801 (2013).
[19] J. W. Wells, J. H. Dil, F. Meier, J. Lobo-Checa, V. N. Petrov, J. Osterwalder, M. M. Ugeda, I. Fernandez-Torrente, J. I. Pascual, E. D. L. Rienks, M. F. Jensen, and Ph. Hofmann, Phys. Rev. Lett. **102**, 096802 (2009).
[20] A. Kühnle, L. M. Molina, T. R. Linderoth, B. Hammer, and F. Besenbacher, Phys. Rev. Lett. **93**, 086101 (2004).
[21] M. Pivetta *et al.* (unpublished).
[22] R. Gaisch, J. K. Gimzewski, B. Reihl, R. R. Schlittler, M. Tschudy, and W. D. Schneider, Ultramicroscopy **42**, 1621 (1992).
[23] K.-M. Ho and K. P. Bohnen, Phys. Rev. Lett. **59**, 1833 (1987).
[24] P. Giannozzi *et al.*, J. Phys.: Condens. Matter **21**, 395502 (2009).
[25] A. Dal Corso and A. Mosca Conte, Phys. Rev. B **71**, 115106 (2005).
[26] S. S. Parihar and P. F. Lyman, J. Vac. Sci. Technol. A **26**, 485 (2008).
[27] L. Lottermoser, T. Buslaps, R. L. Johnson, R. Feidenhans'l, M. Nielsen, D. Smilgies, E. Landenmark, and H. L. Meyerheim, Surf. Sci. **373**, 11 (1997).
[28] W. D. Clendening and C. T. Campbell, J. Phys. Chem. **90**, 6656 (1989).
[29] Y. Liu and R. E. Allen, Phys. Rev. B **52**, 1566 (1995).
[30] D. Kaminski, P. Poodt, E. Aret, N. Radenovic, and E. Vlieg, Surf. Sci. **575**, 233 (2005).
[31] C. Nagl, M. Pinczolits, M. Schmid, P. Varga, and I. K. Robinson, Phys. Rev. B **52**, 16796 (1995).

[32]H. Okamoto and T. B. Massalski, Bull. Alloy Phase Diagrams **4**, 401 (1983).

[33]J. H. Jeon, K. H. Chung, H. Kim, and S.-J. Kahng, Surf. Sci. **603**, 145 (2009).

[34]A. Nuber, M. Higashiguchi, F. Forster, P. Blaha, K. Shimada, and F. Reinert, Phys. Rev. B **78**, 195412 (2008).

[35]C. Tournier-Colletta, L. Cardenas, Y. Fagot-Revurat, B. Kierren, A. Tejeda, D. Malterre, P. Le Fèvre, F. Bertran, and A. Taleb-Ibrahimi, Phys. Rev. B **82**, 165429 (2010).

[36]A. Crepaldi, S. Pons, E. Frantzeskakis, F. Calleja, M. Etzkorn, A. P. Seitsonen, K. Kern, H. Brune, and M. Grioni, Phys. Rev. B **87**, 115138 (2013).

[37]A. Crepaldi, G. Bihlmayer, K. Kern, and M. Grioni, New J. Phys. **15**, 105013 (2013).

[38]A fine inspection of the STM images (5 K) suggests a weak $c(2 \times 8)$ superstructure associated with a slight dimerization of the row atoms. This is only a low-temperature feature and therefore not relevant to the discussion of the ARPES data.